Differential roles of FOXO transcription factors on insulin action in brown and white adipose tissue

Erica P. Homan,[1,2] Bruna B. Brandão,[1] Samir Softic,[1,3] Abdelfattah El Ouaamari,[4,5,6] Brian T. O'Neill,[1,7] Rohit N. Kulkarni,[4] Jason K. Kim,[8,9] and C. Ronald Kahn[1]

[1]Section on Integrative Physiology and Metabolism, Joslin Diabetes Center, Harvard Medical School, Boston, Massachusetts, USA. [2]Biology Department, Northeastern University, Boston, Massachusetts, USA. [3]Division of Gastroenterology, Hepatology and Nutrition, Department of Pediatrics, and Department of Pharmacology and Nutritional Sciences, University of Kentucky College of Medicine, University of Kentucky, Lexington, Kentucky, USA. [4]Section on Islet Cell and Regenerative Biology, Joslin Diabetes Center, Harvard Medical School, Boston, Massachusetts, USA. [5]Division of Endocrinology, Metabolism and Nutrition, Department of Medicine, and [6]The Child Health Institute of New Jersey, Robert Wood Johnson Medical School, Rutgers, The State University of New Jersey, New Brunswick, New Jersey, USA. [7]Fraternal Order of Eagles Diabetes Research Center and Division of Endocrinology and Metabolism, Roy J. and Lucille A. Carver College of Medicine, University of Iowa, Iowa City, Iowa, USA. [8]Program in Molecular Medicine and [9]Division of Endocrinology and Metabolism, Department of Medicine, University of Massachusetts Medical School, Worcester, Massachusetts, USA.

Insulin and IGF-1 are essential for adipocyte differentiation and function. Mice lacking insulin and IGF-1 receptors in fat (FIGIR-KO, fat-specific IGF-1 receptor and insulin receptor–KO) exhibit complete loss of white and brown adipose tissue (WAT and BAT), glucose intolerance, insulin resistance, hepatosteatosis, and cold intolerance. To determine the role of FOXO transcription factors in the altered adipose phenotype, we generated FIGIR-KO mice with fat-specific KO of fat-expressed *Foxo*s [*Foxo1*, *Foxo3*, *Foxo4*] (F-Quint–KO). Unlike FIGIR-KO mice, F-Quint–KO mice had normal BAT, glucose tolerance, insulin-regulated hepatic glucose production, and cold tolerance. However, loss of FOXOs only partially rescued subcutaneous WAT and hepatosteatosis, did not rescue perigonadal WAT or systemic insulin resistance, and led to even more marked hyperinsulinemia. Thus, FOXOs play different roles in insulin/IGF-1 action in different adipose depots, being most important in BAT, followed by subcutaneous WAT and then by visceral WAT. Disruption of FOXOs in fat also led to a reversal of insulin resistance in liver, but not in skeletal muscle, and an exacerbation of hyperinsulinemia. Thus, adipose FOXOs play a unique role in regulating crosstalk between adipose depots, liver, and β cells.

Introduction

Insulin and IGF-1, acting through the insulin receptor (IR) and IGF-1 receptor (IGF1R), are critical hormones in the regulation of metabolism and growth (1). Following ligand binding, these receptors become autophosphorylated and recruit and phosphorylate substrate/adaptor proteins, such as IR substrate 1 (IRS-1), IRS-2, and SHC (2). SHC activates the RAS/MAPK pathway, ultimately leading to increased cell proliferation, while the IRS proteins link to the PI3K/AKT pathway, leading to the regulation of multiple metabolic pathways, including inhibiting gluconeogenesis and apoptosis, while stimulating glucose transport, glycogen synthesis, protein synthesis, gene transcription, and lipid synthesis (2).

In adipose tissue, insulin and IGF-1 are critical for differentiation of preadipocytes, and insulin facilitates glucose uptake and lipid synthesis while inhibiting lipolysis (3). Mice with genetic KO of IR and IGF1R display a nearly complete loss of brown and white adipose tissues throughout life (4). As a result, these mice are unable to maintain their body temperature in the cold, accumulate ectopic lipid in both liver and muscle, and develop severe insulin resistance, glucose intolerance, and pancreatic islet hyperplasia (4, 5). Likewise, inducible deletion of IR and IGF1R in adipocytes results in the rapid loss of both white and brown fat due to increased lipolysis and increased adipocyte apoptosis (6). These observations demonstrated that insulin and IGF-1 signaling play a crucial role in both development and maintenance of brown and white adipose tissue.

One function of insulin/IGF-1 action, mediated via AKT, is the phosphorylation of members of the FOXO family of transcription factors (7). When phosphorylated, FOXOs interact with the 14-3-3 proteins, leading to the proteins' exclusion from the nucleus, thus blocking FOXO-mediated activation of programs governing gluconeogenesis and lipid synthesis (2, 8, 9). In the absence of IR, IGFR, or their ligands, FOXOs accumulate in the nucleus and remain active (7). In liver and muscle, reversing this activation by deletion of *Foxo*s can reverse many of the phenotypes observed in mice lacking IR, IGF1R, or their ligands. For example, mice lacking IR in liver develop severe hepatic insulin resistance with unsuppressed hepatic glucose production, leading to hyperglycemia, hyperinsulinemia, and glucose intolerance (10). Hepatic deletion of *Foxo1* in these mice rescues the insulin resistance and unsuppressed gluconeogenesis (11). Similarly, mice lacking both IR and IGF1R in muscle or with insulin-deficient diabetes display a marked reduction in muscle mass because of increased proteasomal and autophagy-mediated protein degradation (12). Deletion of the muscle-expressed *Foxo*s in the context of lost IR/IGF1R or insulin-deficient diabetes leads to normalization of autophagy

Conflict of interest: The authors have declared that no conflict of interest exists.

Submitted: August 24, 2020; **Accepted:** August 19, 2021; **Published:** August 24, 2021.
Reference information: *J Clin Invest*. 2021;131(19):e143328.
https://doi.org/10.1172/JCI143328.

and a rescue in muscle mass (13, 14). Thus, constitutive activation of FOXOs as a result of loss of insulin and/or IGF-1 signaling explains many metabolic abnormalities.

In the present study, we have explored the role of FOXOs in insulin/IGF-1 action in adipose tissue by determining the effect of fat-specific deletion of the adipose tissue–expressed *Foxo*s (*Foxo1*, *Foxo3*, and *Foxo4*) in combination with deletion of IR and IGF1R. This reveals a differential role of these transcription factors in maintenance of different white and brown fat depots. This also uncovers unique roles of different fat depots in the crosstalk with the liver and in the marked hyperinsulinemia associated with lipodystrophy, pointing to previously unrecognized differential mechanisms of adipose tissue–mediated regulation of systemic metabolism.

Results

Role of IR and IGF1R in adipose development and partial reversal by deletion of Foxo1, -3, and -4. We have previously reported that mice with fat-specific KO of IR and IGF1R have marked lipodystrophy with no detectable white fat and minimal amounts of brown adipose tissue (4). To address the role of downstream FOXO proteins in this phenotype, fat-specific IR (*Insr*), *Igf1r*, as well as *Foxo1*, *Foxo3*, and *Foxo4* quintuple-KO mice (F-Quint–KO) were generated using a Cre recombinase transgene driven by the adiponectin promoter. F-Quint–KO mice were compared with control floxed littermates (CONT) and with new cohorts of fat-specific *Insr* and *Igf1r* double-KO (FIGIR-KO) mice. At 4 weeks of age, CONT mice weighed 16.1 ± 0.5 g, while FIGIR-KO mice weighed only 13.3 ± 0.9 g, reflecting a decrease in fat mass ($P < 0.05$; Supplemental Figure 1A; supplemental material available online with this article; https://doi.org/10.1172/JCI143328DS1). In contrast, the weight of F-Quint–KO mice was similar to CONT (16.8 ± 0.4 g; Supplemental Figure 1A). From weeks 5 to 9, FIGIR-KO mice steadily gained weight, surpassing the controls. This reflected both linear growth and increasing hepatomegaly (see below) (Supplemental Figure 1A; $P < 0.05$). Indeed, despite the absence of all white and most brown fat, dual-energy x-ray absorptiometry (DEXA) analysis revealed similar total body fat in FIGIR-KO mice relative to CONT (Supplemental Figure 1B) because of presence of fatty liver, consistent with previous studies (5). In contrast, F-Quint–KO mice were similar in weight to CONT at 4 weeks of age and grew on a parallel track (Supplemental Figure 1A; $P < 0.05$) but had a 68% reduction in fat relative to CONT ($P < 0.01$) and FIGIR-KO ($P < 0.01$) mice by DEXA (Supplemental Figure 1B). Both FIGIR-KO and F-Quint–KO mice had about a 30% increase in lean mass relative to CONT mice (Supplemental Figure 1C; $P < 0.0001$).

At sacrifice at 12 weeks of age, FIGIR-KO mice had no detectable perigonadal or inguinal (respectively representative of visceral and subcutaneous) white adipose tissue (WAT) and minimal brown adipose tissue (BAT) (Figure 1, A–C). There was also a complete absence of visceral WAT in the F-Quint–KO mice (Figure 1A; $P < 0.0001$), but unlike the FIGIR-KO mice, there was a recovery in the mass of the subcutaneous WAT to about 30% of normal levels (Figure 1B; $P < 0.05$) and full recovery in the mass of the BAT (Figure 1C). Histologically, the recovered subcutaneous WAT in the F-Quint–KO mice was similar in appearance to CONT littermates but did have an approximately 36% decrease in average adipocyte area and a modest increase in lymphocyte infiltration (Figure 1, D and E). The BAT in F-Quint–KO contained a mixture of characteristic brown adipocytes with multilocular lipid droplets and brown adipocytes with larger unilocular fat droplets when compared with those in control littermates (Figure 1F). This brown fat was functional as it restored normal cold-induced thermogenesis. Indeed, in contrast to the FIGIR-KO mice, which failed to maintain their body temperature and dropped to 26.5°C by the end of the 5-hour cold exposure at 6°C, the F-Quint–KO mice maintained their body temperatures similarly to CONT during cold challenge (Figure 1G).

To assess differences in differentiation capacity, white preadipocytes were isolated from the stromovascular fraction of subcutaneous WAT of CONT, double-floxed, and quintuple-floxed mice and subjected to adenoviral Cre–mediated recombination in vitro to generate preadipocytes lacking *Insr* and *Igf1r* (DKO) and preadipocytes lacking *Insr*, *Igf1r*, *Foxo1*, *Foxo3*, and *Foxo4* (QKO). Mirroring the in vivo observations, DKO subcutaneous white preadipocytes failed to differentiate and accumulate lipid, while both CONT and QKO subcutaneous white preadipocytes differentiated normally and showed equal lipid accumulation by Oil Red O staining (Figure 1H). Assessment of the late adipogenic transcriptional markers, peroxisome proliferator–activated receptor γ (*Pparg*) and CCAAT/enhancer-binding protein α (*Cebpa*), by reverse transcriptase quantitative PCR of cells isolated after 4 days of differentiation showed, respectively, 97% and 73% reductions in expression in DKO cells relative to CONT (Supplemental Figure 2A). The expression levels of both *Pparg* and *Cebpa* were fully restored with loss of FOXOs in the QKO cells (Supplemental Figure 2A). The reduction in expression in DKO cells was associated with a 1.7-fold increase in isoproterenol-induced lipolysis relative to WT, and this was normalized in QKO cells (Supplemental Figure 2B). In contrast, the normal increase in insulin-mediated glucose uptake observed in CONT cells was not observed in DKO and QKO cells (Supplemental Figure 2C).

Recovery of glucose homeostasis but worsening of hyperinsulinemia in F-Quint–KO mice. Assessment of glucose homeostasis at 12 weeks of age revealed marked hyperglycemia in FIGIR-KO mice (fed glucose 466 ± 33 vs. 177 ± 5 mg/dL) in contrast with glucose levels near those of controls in the fed state (213 ± 16 mg/dL) in the F-Quint–KO mice (Figure 2A). Similar changes were seen in the fasted state (Figure 2A). An intraperitoneal glucose challenge revealed markedly impaired glucose tolerance in FIGIR-KO mice at all time points, while glucose tolerance in F-Quint–KO mice was similar to controls (Figure 2B). Consistent with severe insulin resistance, fed insulin levels were elevated 25-fold in FIGIR-KO mice compared with controls (Figure 2C; $P < 0.0001$). Surprisingly, the hyperinsulinemia worsened in the F-Quint–KO mice, with a 75-fold increase in insulin levels compared with controls (Figure 2C; $P < 0.0001$). This order of insulin levels persisted in the fasted state with F-Quint–KO greater than FIGIR-KO and greater than CONT (Figure 2C).

To determine whether the increase in serum insulin levels was due to increased secretion versus altered clearance, we assessed C-peptide levels. Like the serum insulin levels, C-peptide levels in F-Quint–KO mice were 4-fold higher than the FIGIR-KO mice in the fed state ($P < 0.0001$) and almost 2 times higher in the fasted state ($P < 0.05$), indicating increased insulin secretion (Figure

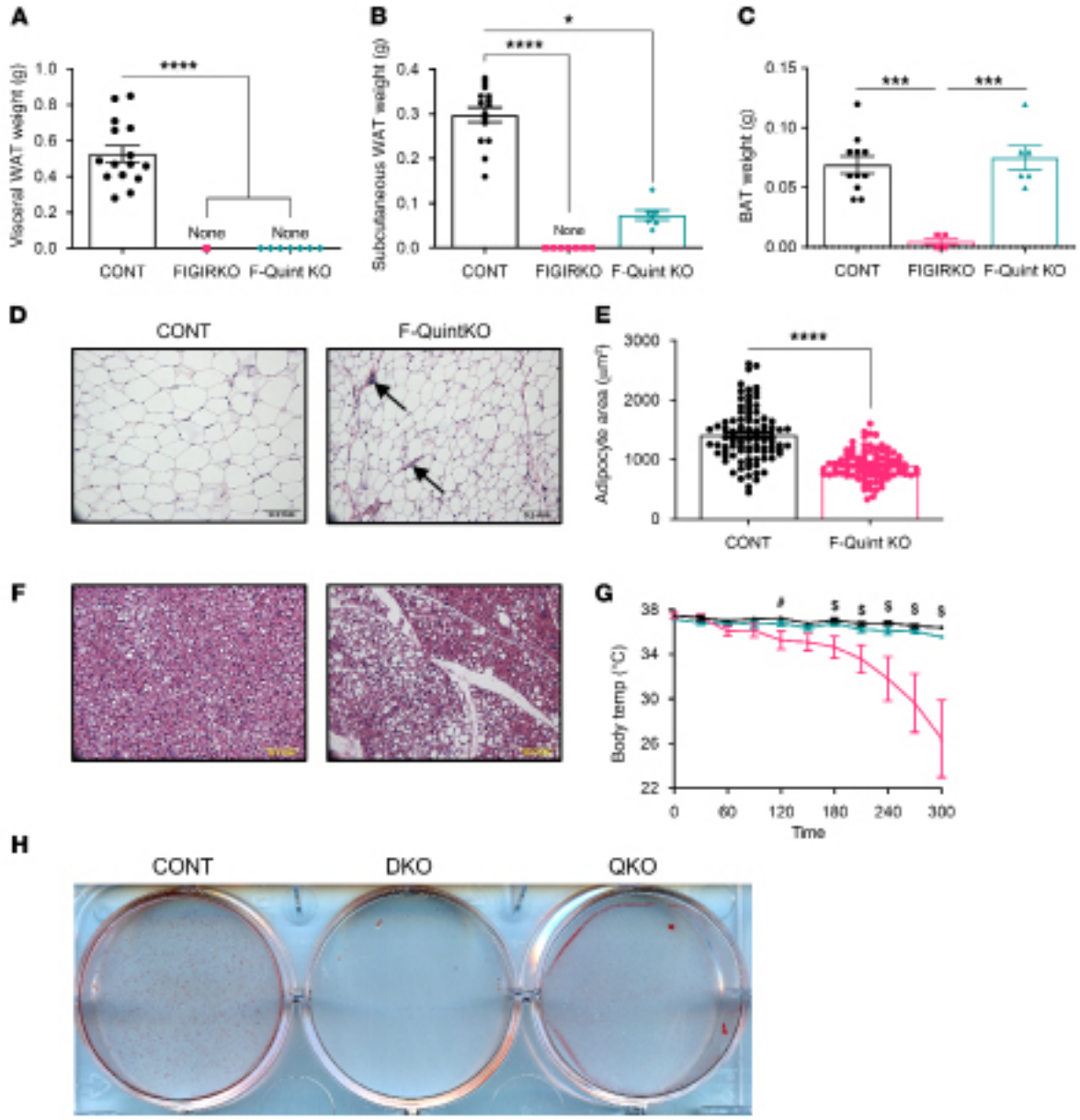

Figure 1. Partial recovery of subcutaneous WAT and recovery of functional BAT with fat-specific deletion of *Foxo1*, *-3*, and *-4* in F-Quint–KO mice. (**A**–**C**) Ad lib–fed CONT, FIGIR-KO, and F-Quint–KO mice were sacrificed at 3 months of age, and visceral (perigonadal) WAT (**A**), subcutaneous (inguinal) WAT (**B**), and BAT (**C**) were removed and weighed. Results represent 4 to 11 mice per group. Statistics were performed using a 1-way ANOVA, where $^{*}P < 0.05$, $^{***}P < 0.001$, and $^{****}P < 0.0001$. (**D**) H&E-stained sections of subcutaneous tissues from the mice in panel **B**. Scale bar: 0.1 mm. Arrows indicate areas of lymphocyte infiltration. (**E**) Average adipocyte area was measured in subcutaneous tissues from mice in panel **B**. Statistics were performed using a 2-way ANOVA, where $^{****}P < 0.0001$. (**F**) H&E-stained sections of BAT tissues from the mice in panel **C**. Scale bar: 0.1 mm. (**G**) Rectal temperature was measured in 3-month-old mice every 30 minutes for 3 hours during exposure to a 6°C environment. Results represent 4 to 11 mice per group. Statistics were performed using a 2-way ANOVA with repeated measures, where $^{\#}P < 0.05$ CONT vs. FIGIR-KO, and $^{\$}P < 0.05$ CONT vs. FIGIR-KO and FIGIR-KO vs. F-Quint–KO. (**H**) Images of subcutaneous adipose–derived CONT, DKO, and QKO adipocyte cell lines stained with Oil Red O after in vitro adipogenic differentiation. Each image is 1 representative well of a 6-well plate.

2D). Insulin resistance, as estimated by the Homeostatic Model Assessment of Insulin Resistance (HOMA-IR), revealed that both the FIGIR-KO and F-Quint–KO mice were markedly insulin resistant (Figure 2E; $P < 0.0001$ and $P < 0.001$, respectively), and this was confirmed by an insulin tolerance test (ITT). FIGIR-KO mice were markedly hyperglycemic compared with controls at the start of the ITT and failed to respond to insulin at all time points (Figure 2F; $P < 0.05$). F-Quint–KO mice, on the other hand, started the ITT at similar glucose levels as controls but like FIGIR-KO mice failed to respond to insulin (Figure 2F; $P < 0.05$). These data indicate that although the loss of *Foxo*s in fat can reverse the hyperglycemia observed in the FIGIR-KO mice, the F-Quint–KO mice remain severely insulin resistant and hyperinsulinemic.

β Cell hyperplasia persists in F-Quint–KO mice. Consistent with the elevated serum levels of insulin and C-peptide, histological examination revealed β cell hyperplasia in both FIGIR-KO and

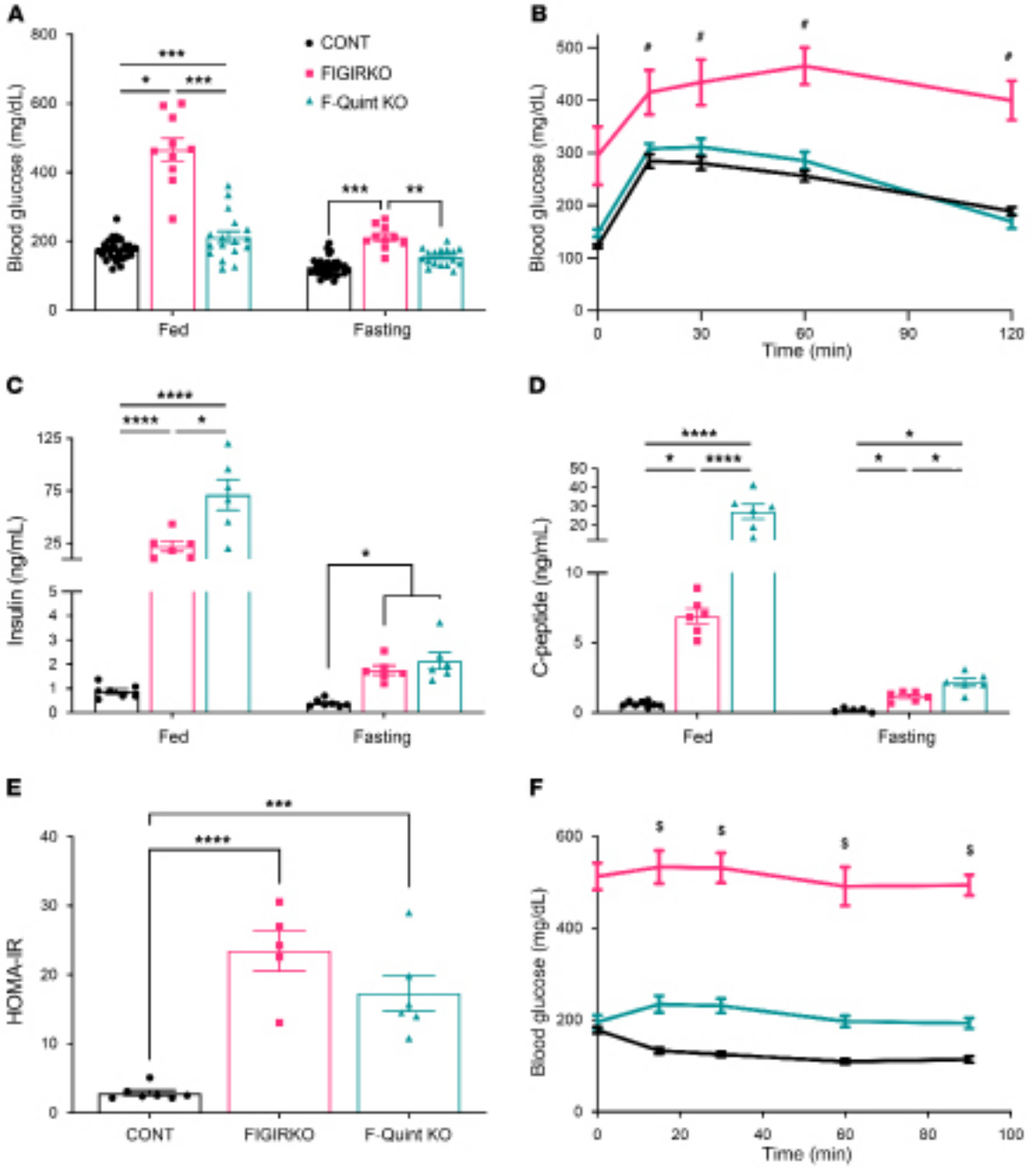

Figure 2. Recovery of glucose homeostasis and worsening of hyperinsulinemia in F-Quint–KO mice. (**A**) Blood glucose in 12-week-old fed and fasting mice. Results represent 10 to 32 mice per group. Statistics were analyzed using a 1-way ANOVA, where $^{*}P < 0.05$, $^{**}P < 0.01$, and $^{***}P < 0.001$. (**B**) Glucose tolerance tests of control, FIGIR-KO, and F-Quint–KO mice at 12 weeks of age. Results represent 5 to 15 mice per group. Statistics were analyzed using a 2-way ANOVA with repeated measures, where $^{\#}P < 0.05$ between CONT vs. FIGIR-KO and FIGIR-KO vs. F-Quint–KO. (**C** and **D**) Serum insulin (**C**) and C-peptide (**D**) levels in the fed or fasted state in 12-week old control, FIGIR-KO, and F-Quint–KO mice. Results represent 6 to 8 mice per group. Statistics were analyzed using a 1-way ANOVA, where $^{*}P < 0.05$, and $^{****}P < 0.0001$. (**E**) HOMA-IR was calculated for CONT, FIGIR-KO, and F-Quint–KO mice at 12 weeks old. Results represent 5 to 7 mice per group. Statistics were analyzed using a 1-way ANOVA, where $^{***}P < 0.001$, and $^{****}P < 0.0001$. (**F**) ITT of CONT, FIGIR-KO, and F-Quint–KO mice at 12 weeks of age. Results represent 5–22 mice per group. Statistics were analyzed using a 2-way ANOVA with repeated measures, where $^{\$}P < 0.05$ between CONT vs. FIGIR-KO, CONT vs. F-Quint–KO, and FIGIR-KO vs. F-Quint–KO.

F-Quint–KO mice relative to CONT (Figure 3A), with a 4.3-fold increase in islet mass in FIGIR-KO mice and a 5-fold increase in F-Quint–KO mice (Figure 3B; $P < 0.05$). This was associated with a 3-fold increase in the percentage of proliferating (Ki67-positive) β cells in both FIGIR-KO and F-Quint–KO mice as compared with controls (Figure 3, A and C; $P < 0.05$). An in vivo glucose-stimulated insulin secretion assay at 6 months of age showed low, but normal, glucose-stimulated insulin secretion (GSIS) in controls, whereas in FIGIR-KO mice, basal insulin levels were modestly elevated, and there was a more robust first and second phase insulin release (Supplemental Figure 3A; $P < 0.05$). F-Quint–KO mice showed even more marked increases in basal insulin levels,

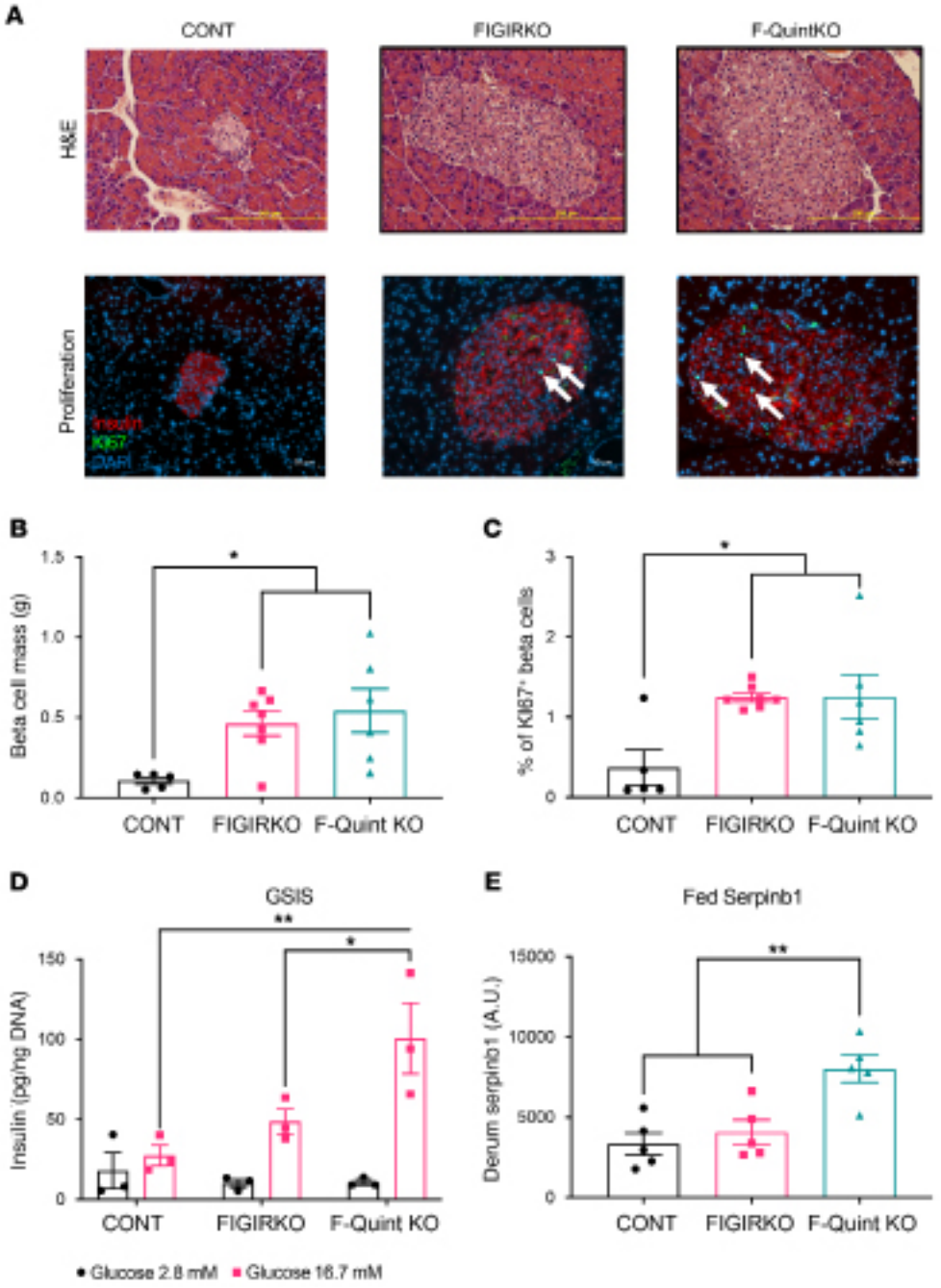

Figure 3. β Cell hyperplasia remains despite loss of *FOXO1*, *-3*, and *-4* in F-Quint–KO mice. (**A**) H&E and immunofluorescence staining for insulin, Ki67, and DAPI in pancreatic sections of CONT, FIGIR-KO, and F-Quint–KO mice at 12 weeks of age. Scale bars: 200 μm for H&E staining and 50 μm for immunofluorescence. White arrows indicate Ki67$^+$ β cells. (**B**) Mass of β cells relative to total pancreas mass and (**C**) the percentage of Ki67$^+$ β cells were measured. Results represent 5–7 mice per group. Statistics were analyzed using a 1-way ANOVA, where $^*P < 0.05$. (**D**) In vitro GSIS results represent 3 per group. Statistics were analyzed using a 2-way ANOVA, where $^*P < 0.05$, and $^{**}P < 0.01$. (**E**) Densitometric quantification of SERPINB1 serum protein levels in the fed state determined by Western blot analysis in 12-week-old mice. Results represent 4 to 5 mice per group. Statistics were analyzed using a 1-way ANOVA, where $^{**}P < 0.01$.

which persisted throughout the glucose stimulation test (Supplemental Figure 3A; $P < 0.05$). Exposure to 16.7 mM glucose produced about a 2-fold increase in insulin secretion in an in vitro GSIS assay carried out on islets isolated from 2-month-old CONT mice. This was increased to a 4.8-fold stimulation of insulin secretion in FIGIR-KO islets and further enhanced in F-Quint–KO islets to greater than a 9.3-fold increase (Figure 3D). Although elevated circulating C-peptide indicated increased insulin secretion, the ratio of serum C-peptide to insulin in the fed state was reduced by 50% in FIGIR-KO and F-Quint–KO mice ($P < 0.01$ and $P < 0.05$, respectively), indicating that reduced insulin clearance may also contribute to the elevation in circulating insulin (Supplemental Figure 3B). In contrast, in the fasted state there was a 2.5-fold increase in the C-peptide/insulin ratio in FIGIR-KO mice relative to CONT, and this ratio was further increased to 3.8-fold in F-Quint–KO mice, indicating increased insulin clearance may contribute to the lower circulating insulin levels in the fasted state (Supplemental Figure 3B; $P < 0.001$). SERPINB1 is a circulating serine protease inhibitor produced mainly in liver and has been previously shown to contribute to increased β cell proliferation in mice with insulin resistance (15). Although there was no difference in the hepatic expression of *Serpinb1* or in fasted serum SERPINB1 levels between CONT and FIGIR-KO mice, we observed a significant 2-fold increase in serum SERPINB1 protein levels in F-Quint–KO mice as compared with CONT, suggesting that SERPINB1 may contribute to the islet hyperplasia observed in these mice (Figure 3E and Supplemental Figure 3, C–F; $P < 0.01$). These and all other uncut gels can be found in the supplemental material.

Partial recovery of serum triglycerides, free fatty acids, and adipokine levels in F-Quint–KO mice. Consistent with their lipodystrophic phenotype (5), there was a significant increase in serum triglycerides in FIGIR-KO mice in both the fed (12.3-fold, $P < 0.0001$) and the fasted (2.6-fold, $P < 0.05$) states (Figure 4A). Deletion of Foxos largely rescued this hypertriglyceridemia despite persistent partial lipodystrophy (Figure 4A). There was also a significant increase in serum FFAs in the FIGIR-KO mice in

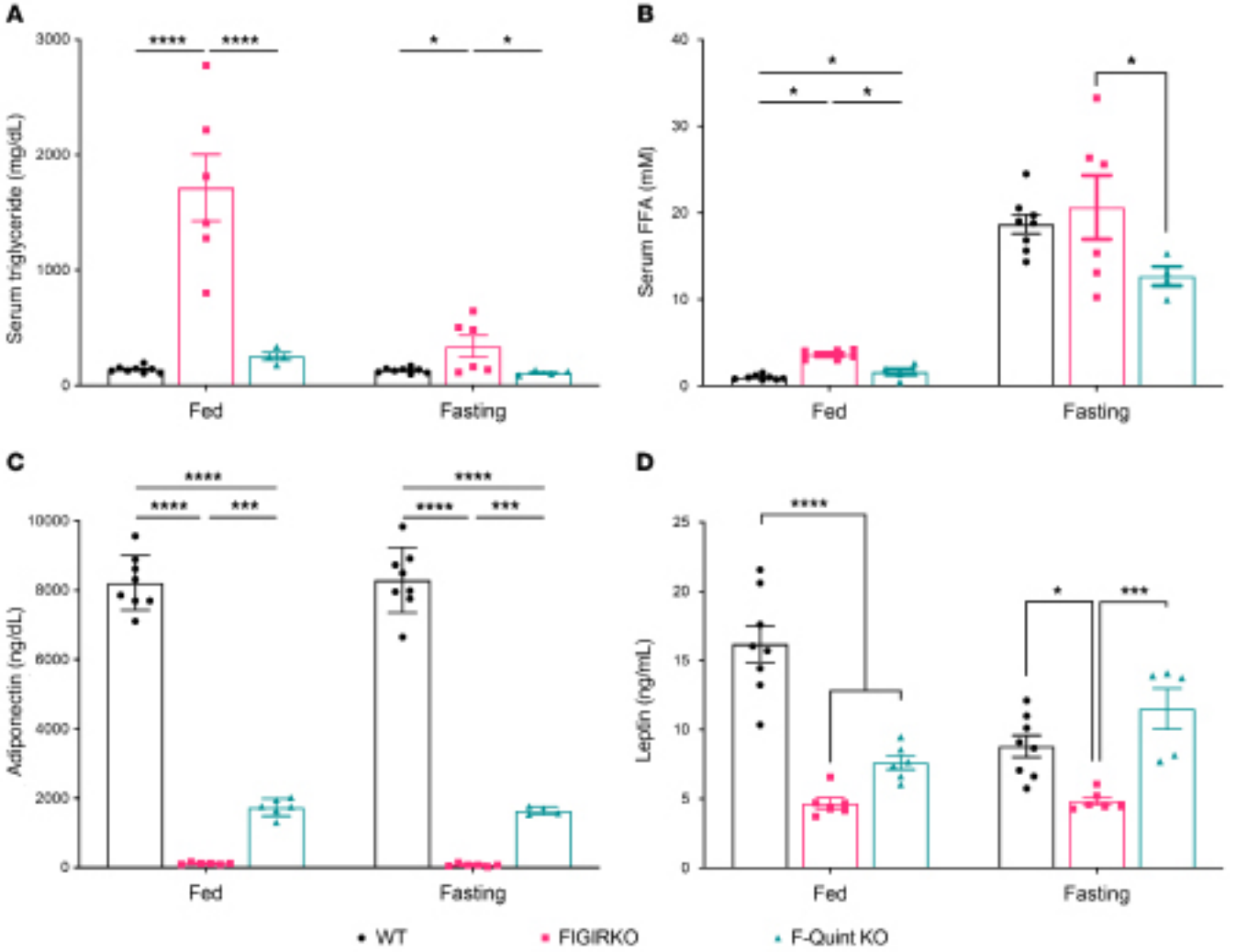

Figure 4. Partial recovery of serum triglyceride, free fatty acid, and adipokine levels in F-Quint–KO mice. (**A**–**D**) Serum triglyceride (**A**), free fatty acid (FFA) (**B**), adiponectin (**C**), and leptin (**D**) were measured as described in Methods in fed and fasting mice at 3 months of age. Results represent 6 to 8 mice per group. Statistics were analyzed using a 1-way ANOVA; where $*P < 0.05$, $***P < 0.001$, and $****P < 0.0001$.

the fed state, which was significantly improved in the F-Quint–KO mice, although serum FFAs remained about 2-fold elevated compared with CONT (Figure 4B; $P < 0.05$). In both the fed and fasting state, there was a marked decrease in adiponectin levels in the FIGIR-KO mice, and this recovered to about 20% of normal levels in the F-Quint–KO mice, paralleling the partial recovery of subcutaneous WAT (Figure 4C; $P < 0.0001$). In the fed state, leptin levels were reduced by approximately 71% and 53% in the FIGIR-KO and F-Quint–KO mice, respectively (Figure 4D; $P < 0.0001$). This was also true for FIGIR-KO mice in the fasted state, whereas fasted F-Quint–KO mice had leptin levels similar to controls (Figure 4D; $P < 0.001$).

Improved food and water intake and fasted energy expenditure in F-Quint–KO mice. Consistent with decreased levels of circulating leptin and diabetic phenotype, FIGIR-KO mice were hyperphagic compared with CONT, with more than a doubling of food intake (Figure 5A) and a parallel increase in water consumption (Figure 5B). Both of these phenotypes were partially rescued in the F-Quint–KO mice (Figure 5, A and B). Energy expenditure assessed using Comprehensive Lab Animal Monitoring Systems (CLAMS) metabolic cages in CONT mice revealed a normal fed-fasted pattern of respiratory exchange ratio (RER), being about 0.9 in the fed state, indicating preferential utilization of carbohydrates, and falling to about 0.7 in the fasted state, consistent with high levels of fat oxidation. This pattern was completely lost in FIGIR-KO, which had stable RER of 0.75 to 0.8 throughout the fed and fasted period (Figure 5C). F-Quint–KO mice had low RER in the fed state ($P < 0.001$), but this dropped during fasting in a manner similar to WT mice (Figure 5C). These differences in RER related to differences in both O_2 consumption and CO_2 production in both FIGIR-KO and F-Quint–KO mice (Supplemental Figure 4, A and B).

Partial rescue of hepatosteatosis with loss of Foxo1, -3, and -4. We have previously shown that FIGIR-KO mice develop severe hepatosteatosis because of their inability to store fat in adipose tissue (5). In the present study, average liver weight in FIGIR-KO mice was 5.7 ± 0.2 g, which was almost 7-fold increased over controls (0.85 ± 0.03 g) (Figure 6A; $P < 0.0001$). This was associated with a 3.1-fold increase in hepatic triglyceride content (Figure 6B; $P <$

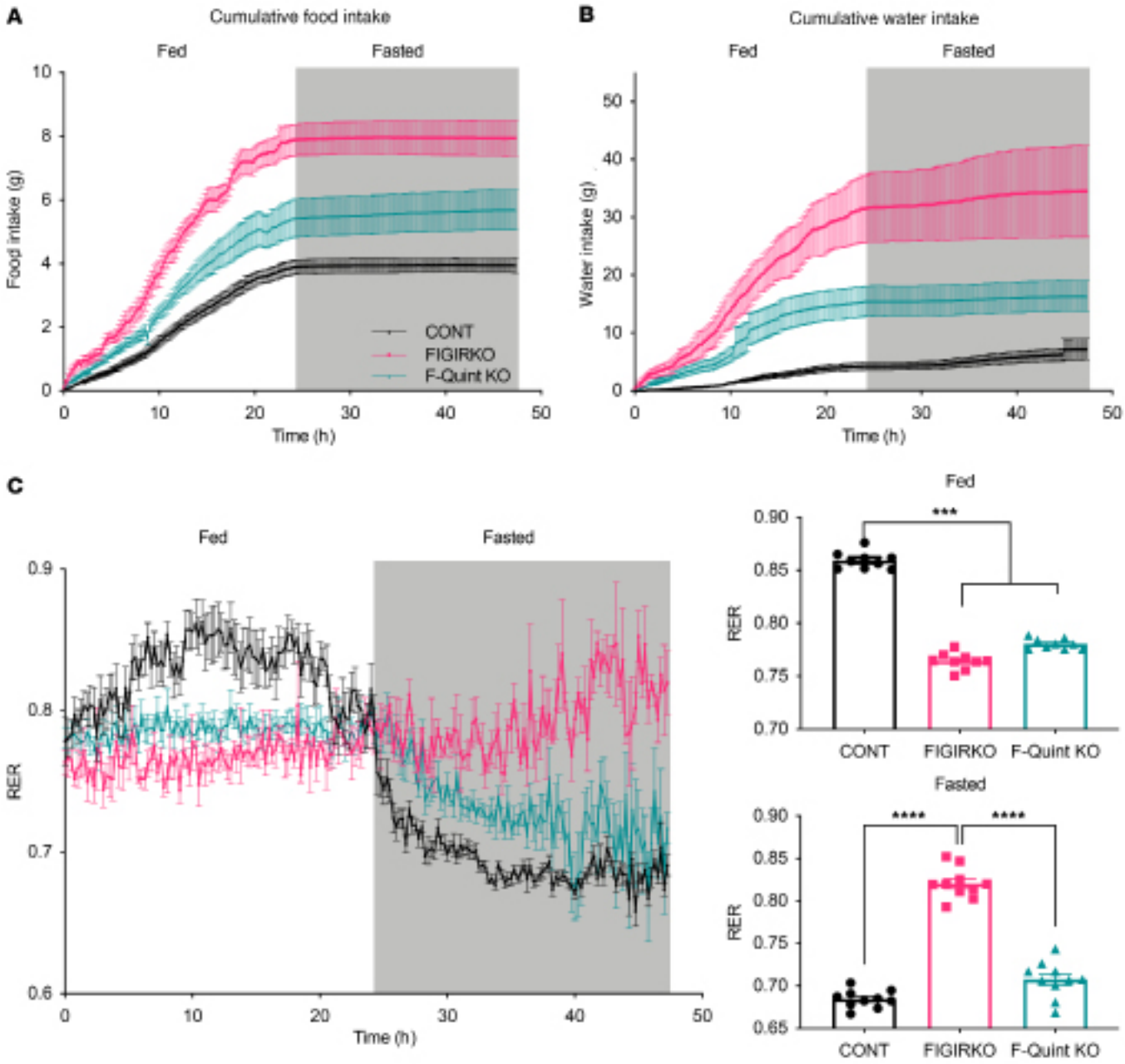

Figure 5. Improvement in food intake and water intake and fasted energy expenditure with loss of *FOXO1*, *-3*, and *-4* in F-Quint–KO mice. (**A**–**C**) Food intake (**A**), water intake (**B**), and RER (**C**) of 12-week-old CONT, FIGIR-KO, and F-Quint–KO mice were measured using CLAMS metabolic cages. Results represent 3–10 mice per group. Statistics were analyzed using a 1-way ANOVA, where ***$P < 0.001$, and ****$P < 0.0001$.

0.0001). Histologically, FIGIR-KO livers exhibited micro- and macrovesicular steatosis throughout the liver (Figure 6C). Compared with FIGIR-KO, liver weights of the F-Quint–KO mice were reduced by 55% but were still 3-fold greater than those of controls (Figure 6A; $P < 0.0001$). In F-Quint–KO mice, there was a proportional decrease in triglyceride content and reduction in steatosis histologically (Figure 6, B and C; $P < 0.0001$).

These histological changes in liver were associated with changes in the expression of gluconeogenic and lipogenic enzymes and markers of inflammation and fibrosis. Thus, there was a 2-fold increase in the expression of glucose-6-phosphatase catalytic subunit (*G6pc*) in livers of the FIGIR-KO mouse, which was reduced in the F-Quint–KO mice to below CONT levels (Figure 6D; $P < 0.0001$). Similarly, expression of *Pck1* and *Fbp1* were increased in FIGIR-KO livers by 1.6- and 2.3-fold, respectively, and were restored to CONT levels in the F-Quint–KO livers (Figure 6D). Interestingly, there was also a 2.1-fold increase in expression of *Pc* in FIGIR-KO liver; however, deletion of *Foxo*s did not rescue this change (Figure 6D; $P < 0.01$). Also, deletion of *Foxo*s did not rescue the increased expression of *Fasn* and *Scd1* observed in FIGIR-KO mice (Figure 6D). Although there was no difference in expression of *Acaca* or *Tnf* among the 3 groups, there was a 12-fold increase in the expression levels of the inflammation marker *Itgax* in FIGIR-KO

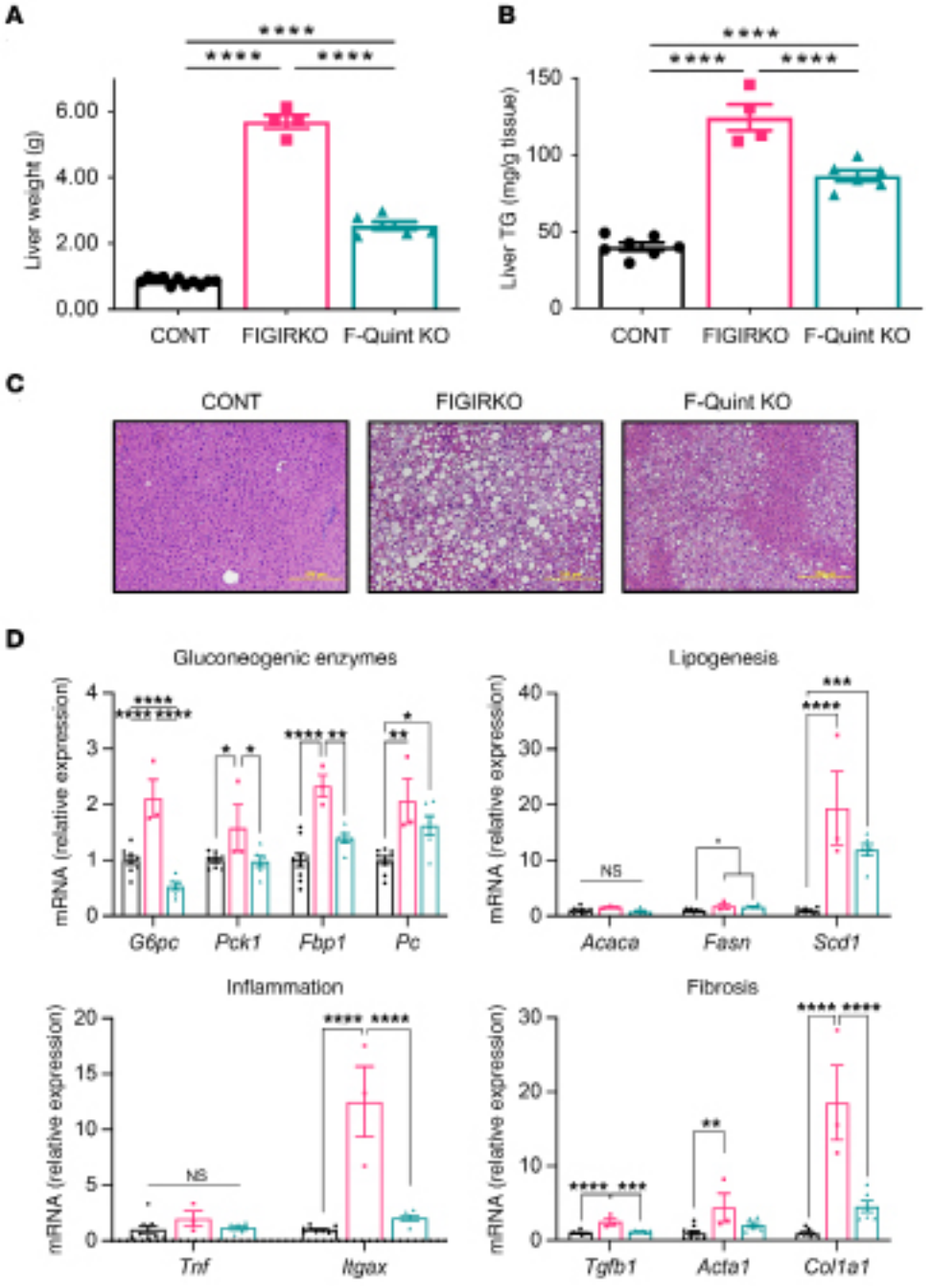

Figure 6. Partial rescue of hepatosteatosis in F-Quint–KO mice. (**A** and **B**) Liver weight (**A**) and liver triglyceride content (mg/g tissue) (**B**) in CONT, FIGIR-KO, and F-Quint–KO mice at 3 months of age. Results represent 4–7 mice per group. Statistics were analyzed using 1-way ANOVA, where ****$P < 0.0001$. (**C**) H&E-stained liver sections from CONT, FIGIR-KO, and F-Quint–KO mice at 3 months of age. Scale bar: 100 μm. (**D**) mRNA expression of genes involved in gluconeogenic enzymes, de novo lipogenesis, inflammation, and fibrosis in the livers of chow-fed CONT, FIGIR-KO, and F-Quint–KO mice at 3 months of age. Results represent 3 to 10 mice per group. Statistics were analyzed using a 1-way ANOVA, where *$P < 0.05$, **$P < 0.01$, ***$P < 0.001$, and ****$P < 0.0001$. *Pck1*, phosphoenolpyruvate carboxykinase 1; *Fbp1*, fructose-bisphosphatase 1; *Pc*, pyruvate carboxylase; *Scd1*, stearoyl-CoA desaturase 1; *Acaca*, acetyl-CoA carboxylase alpha; *Fasn*, fatty acid synthase; *Itgax*, integrin alpha X; *Acta1*, actin, alpha 1, skeletal muscle; *Col1a1*, alpha 1 chain of type I collagen.

livers ($P < 0.0001$), which was rescued in the F-Quint–KO mice (Figure 6D). FIGIR-KO livers also displayed increases in expression levels of *Tgfb1* ($P < 0.0001$), *Col1a1* ($P < 0.01$), and *Acta1* ($P < 0.0001$), when compared with CONT livers, which were rescued in the F-Quint–KO mice (Figure 6D).

Restoration of liver insulin signaling in F-Quint–KO mice. To determine the potential mechanism of the improved metabolic state in F-Quint–KO mice, we assessed liver and muscle insulin sensitivity by in vivo stimulation. In both the basal and stimulated state, there was a 4-fold decrease in the level of IR protein in livers of FIGIR-KO mice relative to CONT ($P < 0.0001$), and this was partially recovered in the F-Quint–KO mice ($P < 0.001$; Figure 7, A and B). Despite the decrease in receptor content, there was a 3-fold increase in the absolute level of basal phosphorylation of the insulin receptor (p-IR) in FIGIR-KO mice relative to CONT, resulting in a 15-fold increase in the ratio of p-IR to IR (Figure 7, A–D; $P < 0.0001$). Response to exogenous insulin, however, was markedly blunted because of downregulation of the receptor. In the F-Quint–KO mice, the increase in basal IR phosphorylation persisted, but there were a more robust increase in the insulin-stimulated phosphorylation and a partial recovery in the level of IR protein, resulting in normalization of the ratio of p-IR to IR when insulin stimulated, whereas basal IR phosphorylation relative to IR protein remained elevated (Figure 7, A–D). A similar increase in basal insulin signaling was observed via increased p-AKT/AKT in FIGIR-KO and F-Quint–KO mice relative to control

(Figure 7, A and E), and following insulin stimulation, there was an increase in p-AKT/AKT in F-Quint–KO livers relative to control and FIGIR-KO livers (Figure 7, A and E). We did not observe any differences in basal or stimulated phosphorylation of ERK1/2 or total ERK1/2 among the 3 groups (Figure 7, A and F), but rather a significant 2-fold increase in Grb2 protein in the F-Quint–KO liver (Figure 7, A and G; $P < 0.001$). There was no difference in the expression of *Insr* mRNA in CONT, FIGIR-KO, and F-Quint–KO livers (Supplemental Figure 5A).

As in liver, insulin signaling in muscle revealed insulin resistance in FIGIR-KO mice, but in this case, there was no recovery in the F-Quint–KO mice. In contrast to the robust increase in p-IR in CONT mice following insulin stimulation ($P < 0.0001$), we observed no increase in insulin-stimulated IR phosphorylation in FIGIR-KO and F-Quint–KO muscle (Figure 7, H and J) and no significant change in total IR protein levels (Figure 7, H and I). There was also no significant change in phosphorylation of AKT or ERK1/2 in response to insulin in FIGIR-KO muscle (Figure 7, H, L, and M). Although there was a recovery in insulin-stimulated phosphorylation of AKT, we observed no recovery in the phosphorylation of ERK1/2 in F-Quint–KO mice (Figure 7, H, L, and M; $P < 0.0001$), and Grb2 protein levels were unchanged (Figure 7, H and N).

To determine the physiological effect of these changes, we performed hyperinsulinemic-euglycemic clamp in awake mice (Supplemental Figure 5B). Relative to CONT, both FIGIR-KO and F-Quint–KO mice were whole-body insulin resistant, as demonstrated by a 75% reduction in the glucose infusion rate during the clamp (Figure 8A; $P < 0.05$). This occurred despite the fact that insulin levels obtained during the clamp were 2-fold higher in FIGIR-KO and F-Quint–KO mice as compared with CONT, consistent with decreased insulin clearance in these mice (Supplemental Figure 5C). Based on tracer infusion, whole-body glucose turnover rates were reduced by 40% in FIGIR-KO mice compared with CONT, and this worsened to a 60% decrease in F-Quint–KO mice (Figure 8B; $P < 0.0001$). Similarly, whole-body glycolysis was decreased by 67% in FIGIR-KO mice relative to CONT ($P < 0.01$) and was reduced further in F-Quint–KO mice ($P < 0.0001$) (Supplemental Figure 5D). Relative to CONT, there was also a 50% decrease in whole-body glycogen plus lipid synthesis in both the FIGIR-KO and F-Quint–KO mice (Figure 8C; $P < 0.01$). Assessment of glycogen synthase kinase-3 (GSK3) levels in liver revealed a significant 1.3-fold increase in FIGIR-KO relative to CONT (Supplemental Figure 6, A and C). No significant difference was detected in GSK3 levels in the livers of F-Quint–KO mice relative to CONT and FIGIR-KO (Supplemental Figure 6, A and C). Expression of the downstream target of GSK3, *glycogen synthase 2* (*Gys2*), in liver was reduced by approximately 50% in FIGIR-KO relative to CONT, and this was fully recovered in F-Quint–KO (Supplemental Figure 6E). Assessment of GSK3 levels in muscle did not reveal any differences between genotypes (Supplemental Figure 6, B and D). There was no difference in insulin-stimulated glucose uptake in skeletal muscle between CONT and FIGIR-KO mice, but this was significantly reduced by 85% in F-Quint–KO mice (Figure 8D; $P < 0.01$). Systemic insulin resistance was also reflected by a 2-fold increase in basal hepatic glucose production in the FIGIR-KO mice and a failure to suppress hepatic glucose production (HGP) during the insulin clamp; both of these parameters reverted toward normal in the F-Quint–KO mice (Figure 8E). Hepatic insulin action, calculated as insulin-mediated percentage suppression of basal HGP, showed a 70% reduction in FIGIR-KO mice relative to CONT, and this was rescued in the F-Quint–KO mice (Figure 8F; $P < 0.0001$). Taken together, the clamp data indicate severe insulin resistance in muscle and liver of FIGIR-KO mice. In F-Quint–KO mice, insulin resistance in liver, but not in skeletal muscle, was selectively reversed.

Discussion

FOXO transcription factors play important roles in insulin action (16). Following insulin stimulation, FOXOs are phosphorylated, bind to 14-3-3 proteins, and are retained in the cytoplasm, while in the absence of insulin/IGF-1 signaling, they are localized in the nucleus, where they are constitutively active (2, 8). In mice lacking insulin and IGF1Rs in liver or muscle, tissue-specific deletion of *Foxo*s can reverse many of the effects of receptor loss at the transcriptional level (11, 13). In the present study, we assessed to what extent deletion of *Foxo*s could reverse the lipodystrophic phenotype observed in mice lacking IR and IGF1R in fat (FIGIR-KO mice) and how this might provide new insights into tissue communication in the altered metabolism of lipodystrophy. We find that deletion of *Foxo*s in the context of absent IR and IGF1R fully restores BAT mass, allows mice to adapt to a cold challenge, and partially restores subcutaneous WAT, resulting in improved hepatosteatosis and liver insulin sensitivity. However, deletion of *Foxo*s has no effect on restoring visceral WAT, does not reverse muscle insulin resistance, and actually exacerbates the severe hyperinsulinemia observed in FIGIR-KO mice. This divergence of rescue effects points to different roles of FOXO proteins in different adipose depots and how each of these depots contributes to the different phenotypes associated with lipodystrophy.

FOXO proteins were first recognized as downstream insulin/IGF-1 signaling in *Caenorhabditis elegans*, such that deletion of Daf-16 (the FOXO homolog) was able to reverse the longevity phenotype observed in worms lacking Daf-2 (the IR/IGF1R homolog; ref. 17). In mice, liver-specific deletion of the IR leads to a wide range of changes in gene expression, increased HGP, and hyperglycemia, and these are largely rescued by deletion of *Foxo1*, the major FOXO protein in the liver (10, 11). Likewise, the major phenotype of muscle-specific deletion of *Insr* and *Igf1r* in mice is a loss in muscle mass because of increased autolysosomal degradation and is largely rescued by *Foxo* deletion (12, 13). In this tissue, however, rescue requires deletion of *Foxo-1*, *-3*, and *-4*, since muscle expresses these 3 FOXO proteins with overlapping functions (13). Also, in this tissue, deletion of *Foxo*s was not sufficient to rescue the abnormal proteasomal activity or the abnormality in insulin-stimulated glucose transport following receptor deletion (13). Adipose tissue shows even more complexity because of its dependence on 3 FOXO proteins as well as the biology of adipose tissue differing greatly from one fat depot to another (18). Thus, creation of an F-Quint–KO mouse completely rescues brown fat mass and function, and partially corrects the loss of subcutaneous white fat, but has virtually no effect on rescuing visceral WAT and some of its functions.

Previous studies have shown that a major role of FOXO1 in fat is to suppress adipogenesis (19). Using the 3T3-F442A preadipo-

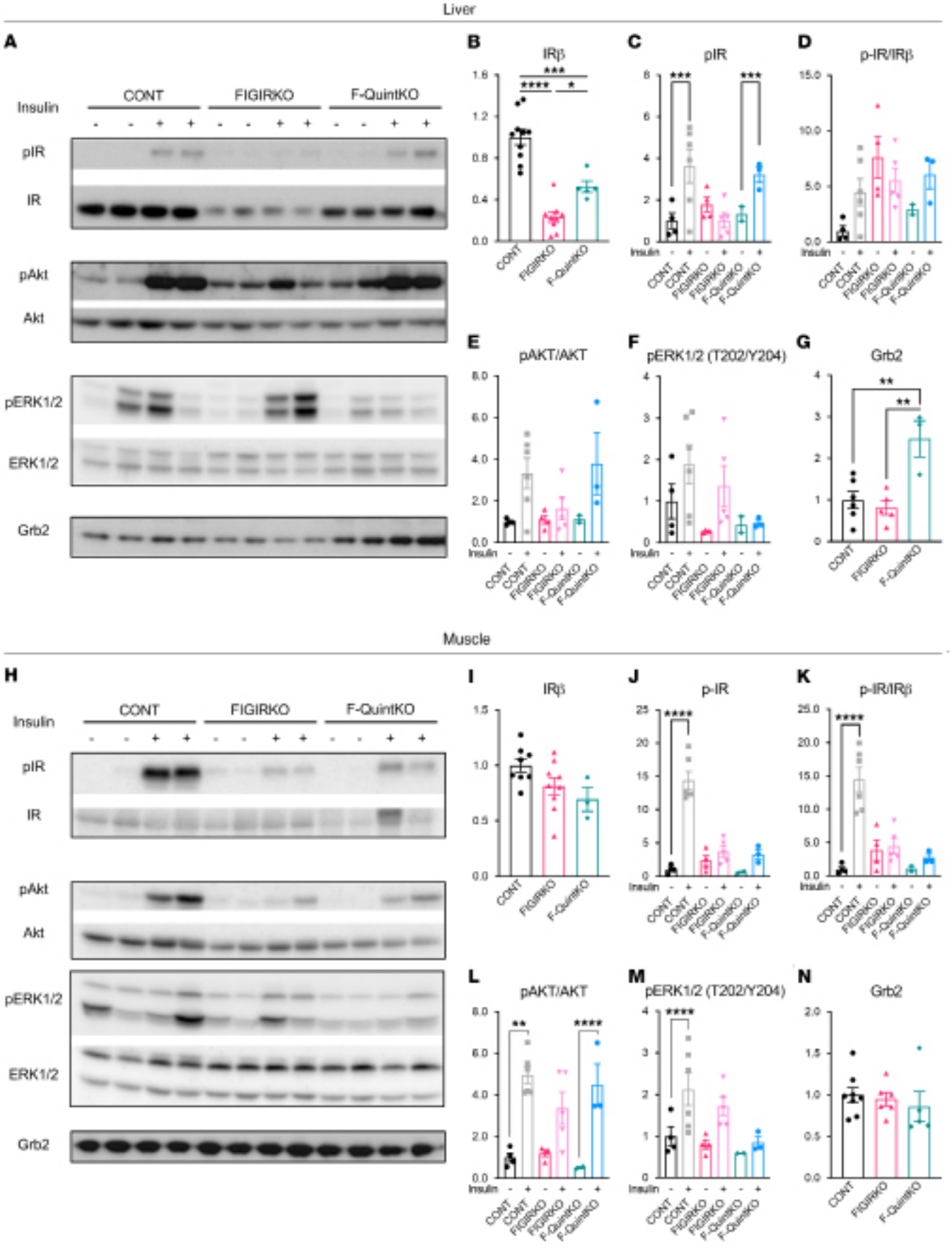
Liver
A
Insulin
CONT
FIGIRKO
F-QuintKO
pIR
IR
pAkt
Akt
pERK1/2
ERK1/2
Grb2
B
IRβ
C
pIR
D
p-IR/IRβ
E
pAKT/AKT
F
pERK1/2 (T202/Y204)
G
Grb2
Muscle
H
I
IRβ
J
p-IR
K
p-IR/IRβ
L
pAKT/AKT
M
pERK1/2 (T202/Y204)
N
Grb2

Figure 7. Restoration of liver insulin sensitivity in the context of whole-body insulin resistance in F-Quint–KO mice. (**A**–**G**) Western blot (**A**) and densitometric quantification of total IR-β (**B**), phosphorylated IR (p-IR) (**C**), p-IR/IR-β (**D**), p-AKT/AKT (**E**), p-ERK1/2 (**F**), and growth factor receptor-bound protein 2 (Grb2) (**G**) in livers of 3-month-old mice. (**H**–**N**) Western blot (**H**) and densitometric quantification of protein levels of total IR-β (**I**), p-IR (**J**), p-IR/IR-β (**K**), p-AKT/AKT (**L**), p-ERK1/2 (**M**), and Grb2 (**N**) in soleus muscles of 3-month-old mice. Results represent 3 to 4 mice per group. Statistics were analyzed using a 1-way ANOVA, where $*P < 0.05$, $**P < 0.01$, $***P < 0.001$, and $****P < 0.0001$.

cyte cell line, Nakae et al. found that FOXO1 binds to the promoter of *Pparg* and inhibits its expression (19). Additionally, through its interaction with PPARγ, FOXO1 blocks the formation of the PPARγ/retinoid X receptor functional complex involved in adipogenesis (20). In preadipocytes lacking IR, IRS proteins, or AKT, there is an increase in FOXO1 activation coupled with impaired differentiation (21). Nakae et al. found that expressing a dominant-negative form of FOXO1 is sufficient to restore adipocyte differentiation from IR-KO embryonic fibroblasts (19). In vitro, we find that KO of *Foxo-1*, *-3*, and *-4* is also able to allow recovery of differentiation in immortalized subcutaneous white preadipocytes derived from mice with KO of *Insr* and *Igf1r*, as demonstrated by the recovery of both Oil Red O staining and expression of the late adipogenic markers (*Pparg* and *Cebpa*). This is consistent with the partial recovery of subcutaneous WAT and full recovery of BAT in vivo. But this does not explain why there is only partial recovery of subcutaneous WAT and no recovery in visceral WAT in the F-Quint mice. Clearly, there must be other insulin-regulated, but FOXO-independent, factors required for normal preadipocyte differentiation in these depots. In addition to FOXOs' ability to suppress adipocyte differentiation, previous work has shown that FOXOs suppress lipogenesis in WAT in part by suppressing phosphoenolpyruvate carboxykinase expression and glycerologenesis, both of which facilitate triglyceride formation (22). One factor may be the effect of loss of IR/IGF1R on the ability of insulin to suppress lipolysis, where overactive FOXOs promote lipolysis by promoting adipose triglyceride lipase expression (23). Loss of FOXOs in F-Quint–KO mice may also help promote the ability to form and store triglycerides in WAT. A recovery in lipolysis was observed in the QKO cells, indicating the WAT that does recover is functional. This is also consistent with the partial restoration of FFA and reduced adipocyte cell size observed in F-Quint–KO mice in the fed state relative to FIGIR-KO and CONT mice.

Although still incompletely understood, recent publications have identified heterogeneity of white adipocytes, both between visceral and subcutaneous adipose depots and even within a single depot (24–27). These different types of white adipocytes exhibit notable differences in the receptor density, affinity, and signal transduction, and levels of expression of different transcription factors, including FOXOs (25). In addition, visceral adipose tissues have high levels of glucocorticoid and androgen receptors (28), while subcutaneous adipocytes have higher estrogen receptor binding (29). Visceral WAT is also more sensitive to catecholamine-stimulated lipolysis than subcutaneous WAT due to an enrichment of β_3-adrenergic receptors, and differences in lipolysis have also been observed between white adipocyte subtypes (25). These differences in receptor signaling and receptor crosstalk can influence adipocyte differentiation in a depot-specific manner and could serve as an explanation for only partial recovery of subcutaneous WAT and no recovery of visceral WAT in the F-Quint–KO mice.

In addition to differences at the receptor level, there are notable differences in the expression of developmental genes in different WAT depots, with *Nr2f1*, *Gpc4*, *Thbd*, *HoxA5*, and *HoxC8* more highly expressed in visceral WAT and *Tbx15*, *Shox2*, *En1*, *Sfrp2*, and *HoxC9* more highly expressed in subcutaneous WAT (30). These developmental genes have been shown to play roles in adipocyte differentiation, in triglyceride accumulation, and in controlling lipolytic rate (30). Important differences have also been observed in the role of growth factors like BMP-2, BMP-4, and BMP-7 in white and brown preadipocyte differentiation (31, 32). One striking feature of this model is the almost complete recovery in BAT relative to the partial recovery of subcutaneous WAT and lack of recovery of visceral WAT. While these differences indicate differential roles of FOXOs in BAT than WAT development, they may also represent some effects of endocrine factors WAT produces, such as leptin and adiponectin, on BAT versus WAT differentiation. Further experiments are needed to determine to what extent these and other factors account for the differences in adipocyte development in different depots in the F-Quint–KO mice.

Another important difference between F-Quint–KO and FIGIR-KO mice is the improvement in hepatosteatosis, hepatic insulin sensitivity, and glucose levels following deletion of *Foxo*s in adipose tissue. Since the KOs are all adipose tissue specific, these effects must be secondary to either metabolic or hormonal crosstalk between fat and other tissues. Previous studies have shown that increasing the function and mass of subcutaneous adipose tissue via treatment with thiazolidinediones or genetic overexpression of adiponectin leads to decreased hepatosteatosis and increased insulin sensitivity, even in the face of obesity or type 2 diabetes (33). This has been mainly attributed to an increase in the ability of fat to store triglycerides, thus reducing hepatic fat accumulation (33). However, in our F-Quint–KO model, there are only partial recovery in subcutaneous WAT mass and partial reversal of hepatic triglyceride accumulation, suggesting other factors contribute to the organ-to-organ crosstalk and improvement in liver metabolism. These most likely represent a change in some adipose-secreted hormones that affect hepatic insulin sensitivity (24).

In addition, recovery of BAT could account for some improvement in glycemia and hepatosteatosis in F-Quint–KO mice. In contrast to WAT, which functions to store excess energy, BAT oxidizes FFAs and glucose to produce heat and thus contributes to whole-body glucose and fatty acid homeostasis (18). Indeed, increasing BAT mass by BAT transplantation to supraphysiological levels can partially reverse the abnormal glucose tolerance observed in high fat diet–fed mice, even under conditions when it does not reduce obesity (34). This positive effect is lost when BAT from Il6-KO mice is utilized in the BAT transplantation, suggesting a role of this cytokine on glucose homeostasis and insulin sensitivity (35). BAT-produced 28. Neuregulin 4 has also been shown to improve obesity-related insulin resistance (36). We demonstrated

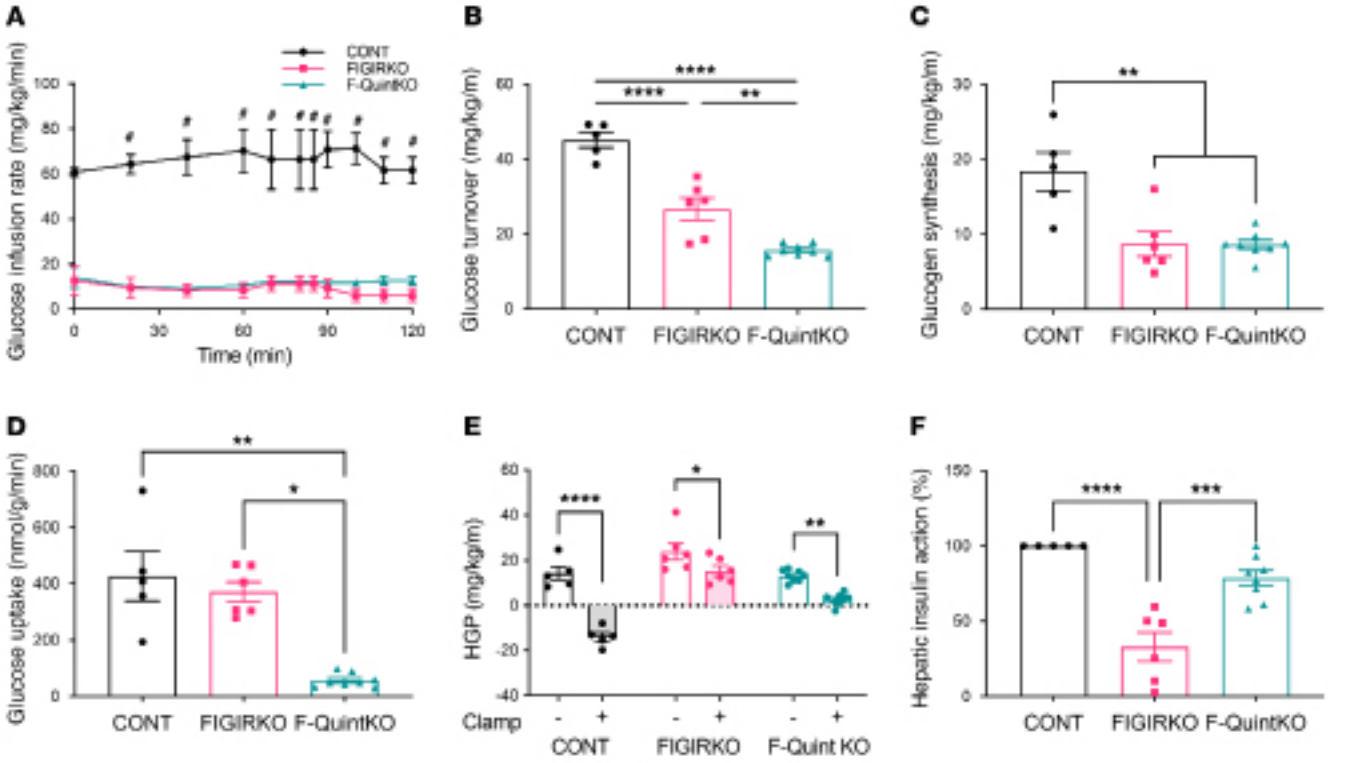

Figure 8. Restoration of liver insulin sensitivity in the context of whole-body insulin resistance in F-Quint–KO mice. (**A**) Glucose infusion rate adjusted every 10 to 20 minutes over the course of a hyperinsulinemic-euglycemic clamp in 3-month-old CONT, FIGIR-KO, and F-Quint–KO mice. Results represent 5 to 8 mice per group. Statistics were analyzed using a 2-way ANOVA with repeated measures, where $^{\#}P < 0.05$ CONT vs. FIGIR-KO and CONT vs. F-Quint–KO. (**B**–**F**) Whole-body glucose turnover (**B**), whole-body glycogen plus lipid synthesis (**C**), insulin-stimulated glucose uptake in skeletal muscle (gastrocnemius) (**D**), basal and clamp HGP (**E**), and hepatic insulin action (**F**) measured during a hyperinsulinemic-euglycemic clamp in 3-month-old CONT, FIGIR-KO, and F-Quint–KO mice. Results represent 5 to 8 mice per group. Statistics were analyzed using a 1-way ANOVA, where $^{*}P < 0.05$, $^{**}P < 0.01$, $^{***}P < 0.001$, and $^{****}P < 0.0001$.

previously that BAT is also a major source of circulating exosomal miRNAs, which have the ability to affect metabolism in many target tissues, including liver (37). Thus, recovery of BAT in the F-Quint–KO mice could account for some of the decrease in serum FFAs and improvement in glucose homeostasis and hepatosteatosis.

Adiponectin is an adipokine involved in regulating glucose levels through its role in enhancing insulin sensitivity by increasing fatty acid oxidation and inhibiting HGP (38, 39). Although all adipose depots make adiponectin, most circulating adiponectin comes from subcutaneous WAT and marrow adipose tissue (40). The partial recovery in serum adiponectin levels observed in the F-Quint–KO mice is likely due to the partial recovery of subcutaneous WAT and could contribute to the improvement in hepatic insulin sensitivity and normalization of hepatic gluconeogenic enzymes but is unlikely to be sufficient to account for the marked improvement observed in the F-Quint–KO mice.

Another interesting aspect of the partial recovery of metabolic defects in F-Quint–KO mice is that despite a recovery in insulin signaling in the liver, as evidenced by enhanced phosphorylation of IR, AKT, and ERK, in the F-Quint–KO mice, there remains severely impaired insulin signaling in muscle, similar in level to that observed in FIGIR-KO mice. This differential insulin resistance is also supported by the clamp data, where liver insulin sensitivity, i.e., the ability of insulin to turn off HGP, is partially recovered in F-Quint–KO mice. Mechanistically, this is also supported by reversal of the increase in the gluconeogenic enzymes, *G6pc*, *Pck1*, *Fbp1*, and *Pc*, observed in the F-Quint–KO livers as compared with FIGIR-KO livers. Despite the markedly improved glucose tolerance phenotype in the F-Quint–KO mice, these mice remain insulin resistant in muscle, as demonstrated by the low glucose infusion rates during the clamp and the decrease in skeletal muscle glucose uptake. Thus, it is likely that the markedly increased insulin secretion in the F-Quint–KO mice and the partial recovery of hepatic insulin action result in the improved glucose tolerance. The cause for the persistent low glucose uptake in skeletal muscle in F-Quint–KO mice is unclear, since AKT phosphorylation, which plays a critical role in insulin-mediated glucose uptake (2), recovered in the soleus muscle of F-Quint–KO mice. Although we did not directly assess PI3K activity, nonesterified fatty acids (NEFAs) can induce a defect in muscle glucose because of impaired PI3K activation (41), and PI3K can act through atypical PKCs and other mechanisms to facilitate glucose uptake (42, 43).

It is well established that insulin action decreases the lipolysis and release of NEFAs and glycerol from WAT and, in turn, promotes gluconeogenesis via hepatic fatty acid oxidation (44). The recovery of some adipose tissue depots in F-Quint–KO mice permits triglyceride storage in WAT, leading to lower free fatty acid levels in the serum. While insulin-mediated inhibition of lipolysis is likely still impaired in F-Quint–KO mice, insulin could potentially suppress lipolysis indirectly via dampening of the central

nervous system and the recovery of circulating serum leptin levels (45). Indeed, as noted above, it is possible that maintained lipolysis and elevated NEFAs and glycerol could contribute to the partial suppression of HGP observed in F-Quint–KO mice.

An even more remarkable aspect of the F-Quint–KO phenotype is the marked hyperinsulinemia in the mice as compared with both FIGIR-KO and control mice. Hyperinsulinemia can be a result of increased insulin secretion and/or decreased insulin clearance (46). With the liver responsible for approximately 80% of insulin clearance (47) and a clear improvement in hepatosteatosis, along with the reduced liver insulin resistance, in the F-Quint–KO mice, one might predict a recovery in the decreased insulin clearance observed in the FIGIR-KO mice in F-Quint–KO mice. However, insulin clearance, as determined by the ratio of C-peptide to insulin, remained decreased in F-Quint–KO mice. Thus, insulin clearance does not account for the extraordinary hyperinsulinemia observed in the F-Quint–KO mice. Instead, we found even more highly enhanced GSIS in the F-Quint–KO mouse compared with the FIGIR-KO mouse, which already had a significant increase ($P = 0.0015$) in β cell mass and insulin secretion. This occurred in spite of any potential effects of glucotoxicity and lipotoxicity on β cell function (4, 48). What stimulates further β cell hyperfunction in F-Quint–KO mice is not clear, but identification of this factor will be of great interest. Previous work has demonstrated that hepatic insulin resistance due to liver-specific KO of the IR results in increased secretion of SERPINB1 and that this contributes to β cell proliferation (15, 49). While F-Quint–KO mice do have a modest increase in SERPINB1 compared with FIGIR-KO mice, it seems unlikely that this could drive such a major increase in β cell proliferation. It seems more likely that recovery in the brown and/or partial recovery of subcutaneous WAT allows for secretion of additional factors that influence pancreatic β cell growth. It is also possible that some FOXO-dependent adipokine functions to suppress islet proliferation and/or insulin secretion, and thus, loss of FOXOs in F-Quint–KO mice reverses this suppression and leads to enhanced insulin secretion. As noted above, previous work from our lab has demonstrated that adipose tissue serves as an important source for circulating exosomal miRNAs and that these miRNAs can influence gene expression in other tissues (37). Thus, it is possible that the recovery of BAT and partial recovery of subcutaneous WAT restore exosomal secretion of one or more miRNAs that have an impact on β cell proliferation, insulin secretion, or peripheral glucose metabolism. Future work identifying these factors is of high priority, since they could provide new approaches to the treatment of both type 1 and type 2 diabetes.

One limitation of this study is that the adiponectin Cre is developmentally expressed, and therefore, the KO occurs in early development. Future experiments using an inducible adiponectin Cre (6) for ablation of IR and IGF1R in combination with Foxo1, -3, and -4 in adult mice could allow us to determine the kinetics of crosstalk between adipose tissue FOXOs and liver and pancreas as well as of glucose homeostasis.

In conclusion, loss of IR and IGF1R in adipose tissue results in severe lipodystrophy and a metabolic syndrome with insulin resistance, fatty liver, and increased circulating triglycerides and FFAs. Deletion of *Foxo-1*, *-3*, and *-4* in adipose tissue of these mice results in the recovery of BAT, and a partial recovery of subcutaneous WAT, but has no effect on visceral WAT. Systemically, this is associated with a recovery in glucose homeostasis and thermogenesis, and an improvement in hepatic insulin signaling and hepatosteatosis, but a lack of improvement in insulin sensitivity in muscle and a worsening of hyperinsulinemia. Thus, FOXO proteins play very different roles in WAT and BAT development and even between different white adipose depots. Their KO uncovers a new level of crosstalk between fat and other tissues in which different adipose depots exert unique effects on systemic glucose metabolism and insulin resistance in muscle versus liver. More importantly, this also demonstrates unique crosstalk between adipose tissue and the β cell response to insulin resistance, opening a pathway for regulation of each of these processes in independent ways.

Methods

Animals, diets, and whole-body energy expenditure. Mice were housed at 20 to 22°C on a 12-hour light/12-hour dark cycle with ad libitum access to water and food (Mouse Diet 9F; PharmaServ). The sources for the alleles used in this study were $Insr^{lox}$ (50), $Igf1r^{lox}$ (51), $Foxo1^{lox}$ (52), $Foxo3^{lox}$ (53), and $Foxo4^{lox}$ (52). FIGIR-KO or F-Quint–KO mice were generated by breeding $Insr^{lox/lox}$ $Igf1r^{lox/lox}$ mice or $Insr^{lox/lox}$ $Igf1r^{lox/lox}$ $Foxo1^{lox/lox}$ $Foxo3^{lox/lox}$ $Foxo4^{lox/lox}$ mice on a C57BL/6 129SvJ genetic background, respectively, with mice carrying Cre recombinase driven by the adiponectin promoter (Adipo-Cre) on a C57BL/6 background. Adipo-Cre–positive males and Adipo-Cre–negative female mice of each genotype were used for final breeding, and breeder pairs of each genotype were replaced simultaneously every 6 months to ensure little or no genetic drift. Male mice were used throughout the study. Control mice from both double- and quintuple-floxed mice showed no physiological differences and were pooled into a single control group (CONT). A Comprehensive Lab Animal Monitoring System (Columbus Instruments) was used to measure whole-body energy expenditure (oxygen consumption, carbon dioxide production, food and water intake) at ambient temperature (~22°C).

Glucose and insulin tolerance tests. Glucose tolerance tests were performed on overnight-fasted mice by injection of dextrose (2 mg/g) intraperitoneally, and blood glucose was measured at 0, 15, 30, 60, and 120 minutes using an INFINITY glucose meter (US Diagnostics). Insulin tolerance tests were performed in 2-hour fasted mice by injection with insulin (1 U/kg i.p.; Humulin R; Eli Lilly and Company). Glucose levels were measured at 0, 15, 30, 60, and 90 minutes postinjection.

In vivo GSIS. Mice were fasted overnight, then injected intraperitoneally with dextrose (3 mg/g body weight). Serum was collected at 0, 2, 5, 10, and 30 minutes, and insulin concentrations were determined using an ultrasensitive mouse insulin ELISA kit following the low range protocol specified by the manufacturer (Crystal Chem Inc., catalog 90080).

In vitro GSIS. In vitro GSIS was assessed as described (54). Briefly, approximately 5×10^5 β cells were washed with Krebs-Ringer buffer (KRB; 128 mM NaCl, 5 mM KCl, 2.7 mM $CaCl_2$, 1.2 mM $MgCl_2$, 1 mM Na_2HPO_4, 1.2 mM KH_2PO_4, 5 mM $NaHCO_3$, 10 mM HEPES, and 0.1% BSA in deionized water), then incubated for 2 hours in 2 mM glucose (MilliporeSigma) in KRB. After incubation, cells were sequentially incubated for 30 minutes each, alternating 2 and 20 mM glucose in KRB then with 30 mM KCl in KRB. The supernatants after each

30-minute incubation were collected, and insulin was quantified using the STELLUX rodent insulin ELISA kit (ALPCO).

Body temperature and cold exposure. Body temperature was measured in 3-month-old mice using a RET-3 rectal probe (Physitemp). The mice were housed individually at an ambient temperature of 6°C, and the temperature was measured every 30 minutes for 3 hours or until the body temperature dropped below 25°C.

Tissue and serum analysis. Body and tissue weights were measured using a Sartorius BP610 Balance. Fed and fasting blood glucose levels were measured using an INFINITY glucose meter. Fed and fasting blood was collected by cheek puncture, and serum was isolated using Microtainer SST tubes (BD) following the protocol recommended by the manufacturer. Fed and fasting insulin, leptin, C-peptide, triglyceride, and FFA levels were determined by ultrasensitive mouse insulin ELISA (Crystal Chem Inc.), mouse leptin ELISA (Crystal Chem Inc.), mouse C-Peptide ELISA (Crystal Chem Inc.), and Free Fatty Acid Quantitation Kit (MilliporeSigma), respectively. Hormones and adipokines were assessed by ELISA. Triglycerides from liver samples were measured with a triglyceride quantification kit (Abnova; ref. 55). Tissues were fixed in formalin, and sections were stained with H&E. mRNA extraction and quantification were performed as previously described (56).

Measurement of β cell proliferation, islet area, and β cell mass. Pancreatic tissue was immunostained using anti-Ki67 (BD Biosciences catalog number 556003) and anti-insulin (Abcam catalog number ab7842) antibodies. Ki67$^+$ β cells were visualized by immunofluorescence microscopy (Carl Zeiss Axio Imager A2) and counted by a blinded observer (49). Insulin-positive cells colocalized with nuclear DAPI and Ki67 immunostaining were counted as proliferating β cells. The percentage β cell area was determined by ImageJ software (NIH) and calculated as insulin-positive area divided by total pancreas area. The β cell mass was calculated as previously described by the product of the overall pancreas weight measured at sacrifice by the percentage of β cells (10).

Subcutaneous preadipocyte isolation, culture, glucose uptake, and lipolysis assays. Preadipocytes were isolated from newborn *Insr*$^{lox/lox}$ *Igf1r*$^{lox/lox}$ mice or *Insr*$^{lox/lox}$ *Igf1r*$^{lox/lox}$ *Foxo1*$^{lox/lox}$ *Foxo3*$^{lox/lox}$ *Foxo4*$^{lox/lox}$ mice by collagenase digestion of subcutaneous WAT and immortalized by infection with retrovirus encoding SV-40 T-antigen followed by selection with 2 μg/mL hygromycin. Immortalized preadipocytes were infected with adenovirus containing GFP to generate a control cell line or GFP-tagged Cre recombinase to generate *Insr/Igf1r* DKO or *Insr/Igf1r/Foxo1/Foxo3/Foxo4* QKO cell lines. GFP-positive cells were sorted by FACS and expanded in DMEM supplemented with 10% heat-inactivated fetal bovine serum (MilliporeSigma), 100 U/mL penicillin, and 100 μg/mL streptomycin (Gibco, Thermo Fisher Scientific) at 37°C in a 5% CO_2 incubator. Oil Red O staining was performed as previously described (57). mRNA extraction and quantification were performed as previously described (25). For lipolysis, 9 days after induction of differentiation, cells were starved for 4 hours in Krebs Ringer Phosphate HEPES Albumin (KRPHA) buffer at 37°C with shaking. After collecting media to measure basal glycerol release, cells were incubated in fresh KRPHA media containing 10 μM isoproterenol for 90 minutes at 37°C before media were collected to assess glycerol release using a colorimetric assay (25). For assessment of glucose uptake, 9 days postinduction of differentiation, adipocytes were serum deprived in DMEM supplemented with 0.25% BSA overnight and then starved in KRB-HEPES (KRBH) for 1 hour at 37°C. Cells were incubated in fresh KRBH with or without 100 nM insulin for 30 minutes before initiation with the addition of 0.1 μCi/mL of ^{14}C-Deoxy-D-glucose for 10 minutes. The reaction was stopped by the addition of unlabeled 200 mM 2-Deoxy-D-glucose. After 3 washes with ice-cold PBS, cells were collected, protein concentration was quantified, and counts of ^{14}C-Deoxy-D-glucose were assessed after cell lysis in RIPA buffer (made in-house).

In vivo insulin stimulation. Mice were fasted overnight (16 hours), and recombinant human insulin (100 IU/mL, 50 μL; Humulin R) or saline was injected via the inferior vena cava after anesthesia with Avertin (150 mg/kg i.p., MilliporeSigma). At 10 minutes postinjection, soleus muscle and liver were collected and flash frozen using liquid nitrogen.

Protein extraction and immunoblot analysis. Tissues were homogenized in RIPA buffer with protease and phosphatase inhibitor cocktail (BioTools). Proteins were separated using SDS-PAGE and transferred to polyvinylidene difluoride membranes (MilliporeSigma). Immunoblotting was performed using the indicated antibodies: pIR (Tyr1135/1136)/IGFR (Tyr1150/1151) (Cell Signaling Technology, 3024), total IR-β (Cell Signaling Technology, 3020), pAKT (Ser473) (Cell Signaling Technology, 9271), total AKT (Cell Signaling Technology, 4685), p44/42 (ERK-1,2) (Thr202/Tyr204) (Cell Signaling Technology, 9101), total p44/42 ERK1/2 (Cell Signaling Technology, 9102), total Grb2 (Cell Signaling Technology, 3972), GSK-3β (Cell Signaling Technology, D5C5Z), vinculin (MilliporeSigma, MAB3574), secondary anti–rabbit IgG (GE Healthcare UK, NA934V), and secondary anti–mouse IgG (GE Healthcare UK, NA931V). Quantification of immunoblots was performed using ImageJ software.

Hyperinsulinemic-euglycemic clamps. At 5 to 6 days prior to the clamp, mice were anesthetized, and an indwelling catheter was placed in the right internal jugular vein. After recovery, mice were fasted overnight and placed in rat restrainers. After an acclimation period, a 2-hour hyperinsulinemic-euglycemic clamp was conducted in awake mice with a primed and continuous infusion of human insulin (150 mU/kg body weight priming followed by 2.5 mU/kg/min; Humulin) (58). To maintain euglycemia, 20% glucose was infused at variable rates during the clamp. Whole-body glucose turnover was assessed via a continuous infusion of [3-^{3}H]-glucose (PerkinElmer). To measure insulin-stimulated glucose uptake in individual organs, 2-deoxy-D-[1-^{14}C]-glucose was administered as a bolus (10 mCi) at 75 minutes after the start of the clamp. Whole-body glycolysis was calculated from the rate of increase in plasma ^3H_2O concentrations from 80 to 120 minutes. Whole-body glycogen plus lipid synthesis was estimated by subtracting whole-body glycolysis from whole-body glucose turnover. At the conclusion of the clamp, mice were anesthetized, and tissues were harvested, snap-frozen in liquid nitrogen, and kept at –80°C until analysis.

Statistics. Data are presented as mean ± SEM. Comparisons between 2 groups were analyzed using an unpaired 2-tailed Student's *t* test. Comparison between more than 2 groups was performed using 1-way ANOVA or 2-way ANOVA with repeated measures followed by post hoc 2-tailed Student's *t* tests, as appropriate. Statistical analysis was performed using GraphPad Prism (Version 7.02). Significance level was set at $^*P < 0.05$, $^{**}P < 0.01$, $^{***}P < 0.001$, and $^{****}P < 0.0001$.

Study approval. All animal protocols were approved by the Institutional Animal Care and Use Committee of the Joslin Diabetes Center

and University of Massachusetts Medical School and were in accordance with NIH guidelines.

Author contributions

EPH designed the research studies, conducted the experiments, acquired and analyzed the data, and wrote the manuscript. BBB, SS, AEO, BTO, RNK, and JKK assisted in the experimental design and in acquiring and analyzing data and helped write the manuscript. CRK designed the study, supervised all work, and helped write the manuscript.

Acknowledgments

This work was supported by NIH grants T32DK007260 (to EPH), R01DK067536 (to RNK), R01DK103215 (to RNK), R01DK031036 (to CRK), and R01DK082659 (to CRK). The clamp study was conducted by the National Mouse Metabolic Phenotyping Center at the University of Massachusetts Medical School funded by an NIH grant (5U2C-DK093000 to JKK). We thank Hye Lim Noh and Sujin Suk for their assistance with the clamp study. We thank Jennifer Hollister-Lock and Gordon Weir for their assistance with the in vitro GSIS assays. We thank Jane Hu for her assistance with quantifying β cell mass and proliferation. We thank Domenico Accili for providing the *Foxo1*-, *Foxo3*-, and *Foxo4*-floxed mice. We thank Mengyao Ella Li and Kristina M. Kriauciunas for their assistance with the insulin signaling analysis. We thank Masaji Sakaguchi and Christie Penniman for their help with conducting in vivo metabolic assays. We thank Allen Clermont and the Animal Physiology Core of the Joslin Diabetes Research Center, which is supported by NIH P30 DK036836 (to Joslin Diabetes Research Center). We thank Dana-Farber Cancer Institute/Harvard Cancer Center in Boston, Massachusetts, for the use of the Rodent Histopathology Core, which provided tissue embedding, sectioning, and H&E-staining services. Dana-Farber Cancer Institute/Harvard Cancer Center is supported in part by a National Cancer Institute Cancer Center Support Grant, NIH 5 P30 CA06516. The graphical abstract was created with BioRender.

Address correspondence to: C. Ronald Kahn, Joslin Diabetes Center, One Joslin Place, Boston, Massachusetts 02215, USA. Phone: 617.732.2635; Email: c.ronald.kahn@joslin.harvard.edu.

1. Boucher J, et al. Insulin and insulin-like growth factor-1 receptors act as ligand-specific amplitude modulators of a common pathway regulating gene transcription. *J Biol Chem*. 2010;285(22):17235–17245.
2. Boucher J, et al. Insulin receptor signaling in normal and insulin-resistant states. *Cold Spring Harb Perspect Biol*. 2014;6(1):a009191.
3. Ghaben AL, Scherer PE. Adipogenesis and metabolic health. *Nat Rev Mol Cell Biol*. 2019;20(4):242–258.
4. Boucher J, et al. Differential roles of insulin and IGF-1 receptors in adipose tissue development and function. *Diabetes*. 2016;65(8):2201–2213.
5. Softic S, et al. Lipodystrophy due to adipose tissue-specific insulin receptor knockout results in progressive NAFLD. *Diabetes*. 2016;65(8):2187–2200.
6. Sakaguchi M, et al. Adipocyte dynamics and reversible metabolic syndrome in mice with an inducible adipocyte-specific deletion of the insulin receptor. *Cell Metab*. 2017;25(2):448–462.
7. Gross DN, et al. The role of FoxO in the regulation of metabolism. *Oncogene*. 2008;27(16):2320–2336.
8. Tzivion G, et al. FoxO transcription factors; Regulation by AKT and 14-3-3 proteins. *Biochim Biophys Acta*. 2011;1813(11):1938–1945.
9. Kamagate A, et al. FoxO1 mediates insulin-dependent regulation of hepatic VLDL production in mice. *J Clin Invest*. 2008;118(6):2347–2364.
10. Michael MD, et al. Loss of insulin signaling in hepatocytes leads to severe insulin resistance and progressive hepatic dysfunction. *Mol Cell*. 2000;6(1):87–97.
11. O-Sullivan I, et al. FoxO1 integrates direct and indirect effects of insulin on hepatic glucose production and glucose utilization. *Nat Commun*. 2015;6:7079.
12. O'Neill BT, et al. Differential role of insulin/IGF-1 receptor signaling in muscle growth and glucose homeostasis. *Cell Rep*. 2015;11(8):1220–1235.
13. O'Neill BT, et al. Insulin and IGF-1 receptors regulate FoxO-mediated signaling in muscle proteostasis. *J Clin Invest*. 2016;126(9):3433–3446.
14. O'Neill BT, et al. FoxO transcription factors are critical regulators of diabetes-related muscle atrophy. *Diabetes*. 2019;68(3):556–570.
15. El Ouaamari A, et al. SerpinB1 promotes pancreatic beta cell proliferation. *Cell Metab*. 2016;23(1):194–205.
16. Barthel A, et al. FoxO proteins in insulin action and metabolism. *Trends Endocrinol Metab*. 2005;16(4):183–189.
17. Ogg S, et al. The Fork head transcription factor DAF-16 transduces insulin-like metabolic and longevity signals in C. elegans. *Nature*. 1997;389(6654):994–999.
18. Gesta S, et al. Developmental origin of fat: tracking obesity to its source. *Cell*. 2007;131(2):242–256.
19. Nakae J, et al. The forkhead transcription factor Foxo1 regulates adipocyte differentiation. *Dev Cell*. 2003;4(1):119–129.
20. van der Vos KE, Coffer PJ. FOXO-binding partners: it takes two to tango. *Oncogene*. 2008;27(16):2289–2299.
21. Tsuchiya K, Ogawa Y. Forkhead box class O family member proteins: the biology and pathophysiological roles in diabetes. *J Diabetes Investig*. 2017;8(6):726–734.
22. Fan W, et al. FOXO1 transrepresses peroxisome proliferator-activated receptor gamma transactivation, coordinating an insulin-induced feed-forward response in adipocytes. *J Biol Chem*. 2009;284(18):12188–12197.
23. Chakrabarti P, Kandror KV. FoxO1 controls insulin-dependent adipose triglyceride lipase (ATGL) expression and lipolysis in adipocytes. *J Biol Chem*. 2009;284(20):13296–13300.
24. Kahn CR, et al. Altered adipose tissue and adipocyte function in the pathogenesis of metabolic syndrome. *J Clin Invest*. 2019;129(10):3990–4000.
25. Lee KY, et al. Developmental and functional heterogeneity of white adipocytes within a single fat depot. *EMBO J*. 2019;38(3):e99291.
26. Ramirez AK, et al. Single-cell transcriptional networks in differentiating preadipocytes suggest drivers associated with tissue heterogeneity. *Nat Commun*. 2020;11(1):2117.
27. Min SY, et al. Diverse repertoire of human adipocyte subtypes develops from transcriptionally distinct mesenchymal progenitor cells. *Proc Natl Acad Sci U S A*. 2019;116(36):17970–17979.
28. Wajchenberg BL. Subcutaneous and visceral adipose tissue: their relation to the metabolic syndrome. *Endocr Rev*. 2000;21(6):697–738.
29. Davis KE, et al. The sexually dimorphic role of adipose and adipocyte estrogen receptors in modulating adipose tissue expansion, inflammation, and fibrosis. *Mol Metab*. 2013;2(3):227–242.
30. Schoettl T, et al. Heterogeneity of adipose tissue in development and metabolic function. *J Exp Biol*. 2018;221(pt suppl 1):jeb162958.
31. Tseng YH, et al. New role of bone morphogenetic protein 7 in brown adipogenesis and energy expenditure. *Nature*. 2008;454(7207):1000–1004.
32. Schulz TJ, Tseng YH. Emerging role of bone morphogenetic proteins in adipogenesis and energy metabolism. *Cytokine Growth Factor Rev*. 2009;20(5-6):523–531.
33. Kadowaki T, et al. Adiponectin and adiponectin receptors in insulin resistance, diabetes, and the metabolic syndrome. *J Clin Invest*. 2006;116(7):1784–1792.
34. Stanford KI, et al. A novel role for subcutaneous adipose tissue in exercise-induced improvements in glucose homeostasis. *Diabetes*. 2015;64(6):2002–2014.
35. Stanford KI, et al. Brown adipose tissue regulates glucose homeostasis and insulin sensitivity. *J Clin Invest*. 2013;123(1):215–223.
36. Bluher M. Neuregulin 4: a "hotline" between brown fat and liver. *Obesity (Silver Spring)*. 2019;27(10):1555–1557.

37. Thomou T, et al. Adipose-derived circulating miRNAs regulate gene expression in other tissues. *Nature*. 2017;542(7642):450–455.
38. Berg AH, et al. The adipocyte-secreted protein Acrp30 enhances hepatic insulin action. *Nat Med*. 2001;7(8):947–953.
39. Stern JH, et al. Adiponectin, leptin, and fatty acids in the maintenance of metabolic homeostasis through adipose tissue crosstalk. *Cell Metab*. 2016;23(5):770–784.
40. Wang GX, et al. The brown fat secretome: metabolic functions beyond thermogenesis. *Trends Endocrinol Metab*. 2015;26(5):231–237.
41. Kruszynska YT, et al. Fatty acid-induced insulin resistance: decreased muscle PI3K activation but unchanged Akt phosphorylation. *J Clin Endocrinol Metab*. 2002;87(1):226–234.
42. Liu XJ, et al. Atypical protein kinase C in glucose metabolism. *Cell Signal*. 2006;18(12):2071–2076.
43. Standaert ML, et al. Cbl, IRS-1, and IRS-2 mediate effects of rosiglitazone on PI3K, PKC-lambda, and glucose transport in 3T3/L1 adipocytes. *Endocrinology*. 2002;143(5):1705–1716.
44. Petersen MC, et al. Regulation of hepatic glucose metabolism in health and disease. *Nat Rev Endocrinol*. 2017;13(10):572–587.
45. Scherer T, et al. Brain insulin controls adipose tissue lipolysis and lipogenesis. *Cell Metab*. 2011;13(2):183–194.
46. Sechi LA, et al. Insulin hypersecretion: a distinctive feature between essential and secondary hypertension. *Metabolism*. 1992;41(11):1261–1266.
47. Najjar SM, Perdomo G. Hepatic insulin clearance: mechanism and physiology. *Physiology (Bethesda)*. 2019;34(3):198–215.
48. Robertson RP, et al. Beta-cell glucose toxicity, lipotoxicity, and chronic oxidative stress in type 2 diabetes. *Diabetes*. 2004;53 Suppl 1:S119–S124.
49. El Ouaamari A, et al. Liver-derived systemic factors drive beta cell hyperplasia in insulin-resistant states. *Cell Rep*. 2013;3(2):401–410.
50. Bruning JC, et al. A muscle-specific insulin receptor knockout exhibits features of the metabolic syndrome of NIDDM without altering glucose tolerance. *Mol Cell*. 1998;2(5):559–569.
51. Holzenberger M, et al. A targeted partial invalidation of the insulin-like growth factor I receptor gene in mice causes a postnatal growth deficit. *Endocrinology*. 2000;141(7):2557–2566.
52. Paik JH, et al. FoxOs are lineage-restricted redundant tumor suppressors and regulate endothelial cell homeostasis. *Cell*. 2007;128(2):309–323.
53. Castrillon DH, et al. Suppression of ovarian follicle activation in mice by the transcription factor Foxo3a. *Science*. 2003;301(5630):215–218.
54. Pagliuca FW, et al. Generation of functional human pancreatic β cells in vitro. *Cell*. 2014;159(2):428–439.
55. Debosch BJ, et al. Glucose transporter 8 (GLUT8) mediates fructose-induced de novo lipogenesis and macrosteatosis. *J Biol Chem*. 2014;289(16):10989–10998.
56. Boucher J, et al. Impaired thermogenesis and adipose tissue development in mice with fat-specific disruption of insulin and IGF-1 signalling. *Nat Commun*. 2012;3:902.
57. Lee KY, et al. The differential role of Hif1β/Arnt and the hypoxic response in adipose function, fibrosis, and inflammation. *Cell Metab*. 2011;14(4):491–503.
58. Kim JK. Hyperinsulinemic-euglycemic clamp to assess insulin sensitivity in vivo. *Methods Mol Biol*. 2009;560:221–238.